Electronic structure and jumping magnetization of quantum wells in tilted magnetic fields

1991 J. Phys.: Condens. Matter 3 8237

(http://iopscience.iop.org/0953-8984/3/42/018)

J. Phys.: Condens. Matter 3 (1991) 8237–8246. Printed in the UK

Electronic structure and jumping magnetization of quantum wells in tilted magnetic fields

G Marx and R Kümmel

Physikalisches Institut der Universität Würzburg, D-8700 Würzburg, Federal Republic of Germany

Received 25 February 1991

Abstract. The energy spectrum, the density of states, the electron probability distributions and the magnetization of a $Ga_{1-x}Al_xAs$–GaAs–$Ga_{1-x}Al_xAs$ quantum well in strong tilted magnetic fields $\boldsymbol{B} = (B_x, 0, B_z)$ are calculated. It is shown that the spectrum and the probability densities of the states bound in the quantum well would change little if the coupling Hamiltonian $\simeq B_xB_z$ were to be neglected. Localized states appear above the barrier edge. The magnetization parallel to the layer interfaces exhibits oscillations and sharp jumps as a function of the chemical potential. It remains to be seen whether these jumps may serve as the basis for a dissipation free switching device.

1. Introduction

Recent investigations of the energy spectrum and the magnetization of quantum wells (QWs) in high magnetic fields oriented parallel to the interfaces showed the existence of localized states and oscillations of the magnetization as a function of the chemical potential [1, 2], see also [3, 4]. Localization occurs in the barrier for certain values of the (quasi-)continuous momentum $\hbar k_y$ of motion parallel to the interfaces and perpendicular to the field. Since the total energy varies continuously with k_y no energy gaps separate the localized barrier states from the delocalized ones. Therefore, it will be quite impossible to achieve a stable overpopulation of these states which might be desirable for a magnetically tunable laser. However, if a magnetic field component B_z normal to the interfaces is present, and if one takes into account size quantization due to the finite width of the heterojunction, one may have degenerate localized states in the barriers, or at the rim of the effective total potential, separated by energy gaps from the neighbouring states. This can be concluded from the energy spectra and charge density distributions computed in this article for various tilt angles ϑ of the magnetic field $\boldsymbol{B}$. Furthermore, we compute the x-component of the magnetization as a function of the chemical potential and interpret its oscillations and discontinous jumps with the help of the energy spectrum.

2. Method

We consider a $Ga_{1-x}Al_xAs$–GaAs–$Ga_{1-x}Al_xAs$ heterojunction of total width $2L_z$. The GaAs layer extends between $-a/2 < z < a/2$. We model the system by a scalar

0953-8984/91/428237+10$03.50

potential $U(z)$ with $U(z) = 0$ for $|z| < a/2$, $U(z) = V$ for $a/2 < |z| < L_z$ and $U(z) = \infty$ for $|z| > L_z$. The tilted magnetic field is $\boldsymbol{B} = \boldsymbol{e}_x B\cos\vartheta + \boldsymbol{e}_z B\sin\vartheta$. For the vector potential we choose a gauge such that $\boldsymbol{A} = \boldsymbol{e}_y(xB\sin\vartheta - zB\cos\vartheta)$.

For the envelope wavefunction in the effective mass approximation we make the *ansatz* $\Psi(x,y,z) = (1/\sqrt{2\pi})\exp\{ik_y y\}\psi(x,z)$. After substituting x by $x + x_0$ where $x_0 := -\hbar k_y/eB\sin\vartheta$ we obtain the Schrödinger equation

$$(H_x + H_{xz} + H_z)\psi(x,z) = E\psi(x,z). \tag{1}$$

The three components of the total Hamiltonian are

$$H_x = -\frac{\hbar^2}{2m}\frac{\partial^2}{\partial x^2} + P(x) \tag{2}$$

with

$$P(x) = \frac{(eB)^2}{2m}x^2\sin^2\vartheta$$

being the harmonic oscillator potential due to B_z.

$$H_z = -\frac{\hbar^2}{2m}\frac{\partial^2}{\partial z^2} + U_{\text{eff}}(z) \tag{4}$$

with

$$U_{\text{eff}}(z) = \frac{(eB)^2}{2m}z^2\cos^2\vartheta + U(z) \tag{5}$$

being the superposition of the QW potential and the harmonic oscillator potential due to B_x. The coupling Hamiltonian

$$H_{xz} = -\lambda 2\frac{(eB)^2}{2m}z\cos\vartheta x\sin\vartheta \tag{6}$$

couples the motion in the harmonic oscillator potential $P(x)$ of H_x, with the motion in the effective potential $U_{\text{eff}}(z)$ of H_z. If we had a *parabolic* QW potential $U(z)$, equation (1) could be decoupled by a suitable coordinate transformation [5]. This cannot be done in our case of a rectangular QW. Therefore, λ has been introduced formally into equation (6) in order to analyse the influence of H_{xz}: if H_{xz} is taken into acount $\lambda = 1$, and if H_{xz} is neglected $\lambda = 0$. Since k_y does not appear explicitly in equation (1), we get the same eigenvalues for different k_y, i.e. each eigenvalue has a degeneracy (per unit area) which turns out to be $eB\sin\vartheta/2\pi\hbar$.

The calculation of the eigenfunctions and eigenstates is done in two steps:

(i) First we set $\lambda = 0$ in H_{xz} in equation (6). Then we can separate equation (1) and solve

$$H_x\eta_l(x) = E_l^x\eta_l(x) \tag{7}$$

by the harmonic oscillator eigenfunctions $\eta_l(x)$ with the eigenvalues

$$E_l^x = \left(l - \frac{1}{2}\right)\hbar\frac{eB}{m}\sin\vartheta \qquad l = 1,2,3\ldots. \tag{8}$$

In order to solve

$$H_z\varphi_n(z) = E_n^z\varphi_n(z) \qquad n = 1, 2, 3 \ldots \tag{9}$$

we develop its eigenfunctions $\varphi_n(z)$ in terms of the (trigonometric) eigenfunctions of an infinite potential well of width $2L_z$. Thus, we obtain a representation of H_z by matrix elements formed with the trigonometric functions. This matrix is being transformed into a tridiagonal matrix by the Lanczos method [6] and finally diagonalized numerically.

(ii) In the second step we set $\lambda = 1$ and take the functions $\eta_l(x)$ and $\varphi_n(z)$ as the complete basis for the expansion of the solution $\psi(x, z)$ of equation (1):

$$\psi(x, z) = \sum_{nl} a_{ln}\eta_l(x)\varphi_n(z). \tag{10}$$

The advantage of this procedure is that H_x and H_z are already diagonal, whereas H_{xz} can be arranged into a band matrix and diagonalized easily.

For the numerical calculations the Schrödinger equation (1) is written in dimensionless coordinates $(\tilde{x}, \tilde{z}) = (x/a, z/a)$, energies $\tilde{E} = E2ma^2/\hbar^2$, potentials $\tilde{V} = V2ma^2/\hbar^2$, and fields $\tilde{B} = Bea^2/\hbar$. Thus the spectrum obtained for one set of parameters B and a has exactly the same structure as the spectrum for a second set of parameters B' and a' if

$$\frac{B}{B'} = \left(\frac{a'}{a}\right)^2. \tag{11}$$

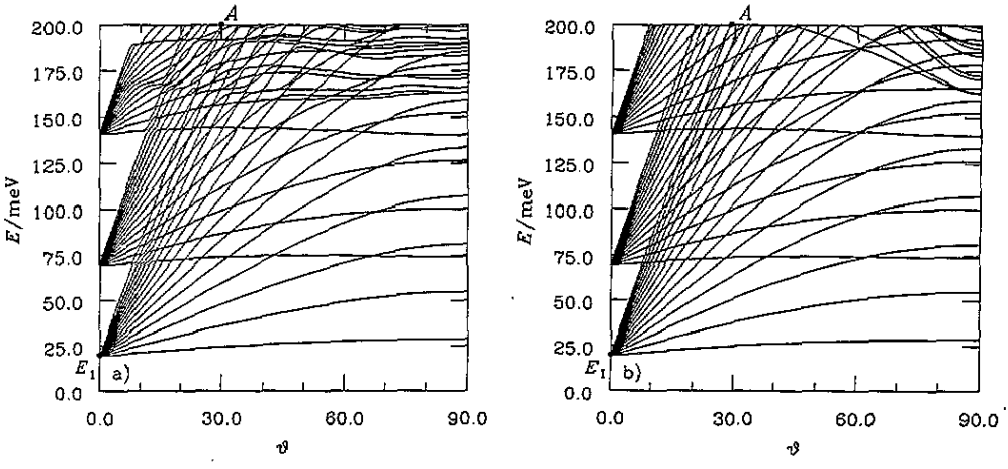

Figure 1. (*a*) Energy spectrum of an isolated $Ga_{0.8}Al_{0.2}As$–GaAs–$Ga_{0.8}Al_{0.2}As$ QW in a magnetic field $B = 15$ T (for $\lambda = 1$) as a function of the tilt angle ϑ. (To the left of the line E_1–A states are missing, see text.) (*b*) Energy spectrum for the same situation as in (*a*), but the coupling Hamiltonian H_{xz} is neglected ($\lambda = 0$).

3. Energy spectrum and density of states

We assume the following GaAs–$Ga_{1-x}Al_xAs$ QW parameters: The well width is $a = 15$ nm, the band-offset is 60%, and $x = 0.20$ so that the potential height is $V = 147$ meV [7]. An effective mass $m = 0.0665\,m_0$ is assumed, m_0 is the free electron mass. For these parameters and for $B = 15$ T we get the energy spectra shown in figures 1(a) and (b) where the spin splitting is neglected. According to equation (11) these are also the spectra for, e.g., $a' = 20$ nm, $B' = 8.4$ T, or $a'' = 25$ nm, $B'' = 5.4$ T, if the energy scale is multiplied by $(a/a')^2$ or $(a/a'')^2$. For the sake of clarity figures 1(a) and (b) only show the tilt angle dependence of those energy levels which evolve from the 15 lowest states of the quasi-continuum in each of the first three sub-bands at tilt angle $\vartheta = 0°$. (Thus, the energy spectrum is incomplete to the left of the straight line joining the points E_1 and A in figures 1(a) and (b).) In figure 1(b) where $\lambda = 0$ eliminates the coupling Hamiltonian H_{xz} from equation (1) the sub-band quantum numbers n and the harmonic oscillator quantum numbers l are good quantum numbers for the problem. n counts the energy levels at $\vartheta = 0°$; l labels the branches of the Landau fans which open up from each sub-band with increasing tilt angle as the magnetic field orientation shifts from parallel to the interfaces to perpendicular to them. The decrease in the lowest sub-band energies with ϑ, which is stronger the higher the sub-band, is due to the reduction of $U_{\text{eff}}(z)$ with decreasing $B\cos\vartheta$. (At $\vartheta = 90°$ where $U_{\text{eff}}(z) = V$ for $a/2 < |z| < L_z$ and $U_{\text{eff}}(z) = \infty$ for $|z| > L_z$ we have the spectrum of a finite well in an infinitely deep well.) In the spectrum of figure 1(a) where $\lambda = 1$, the effect of the coupling by H_{xz} is essentially a lowering of the $E(\vartheta)$ curves and level repulsions at higher energies. The maximum deviation from the $\lambda = 0$ spectrum occurs at a tilt angle of $\vartheta = 45°$, where the coupling Hamiltonian H_{xz} is at a maximum. With increasing distance of ϑ from 45° the coupling becomes less and less important and the energy branches of figures 1(a) and (b) become more and more similar. Thus, for energies $E < V$ neglect of the bothersome H_{xz} in equation (1) can be a reasonable approximation to start with in more complicated calculations, e.g. of many-body effects. This also becomes plausible from comparing the total potential

$$W(x,z,\vartheta) = \frac{(eB)^2}{2m}(x^2\sin^2\vartheta - \lambda 2x\sin\vartheta z\cos\vartheta + z^2\cos^2\vartheta) + U(z) \tag{12}$$

for $\lambda = 1$, figure 2(a), with that for $\lambda = 0$, figure 2(b). The relative unimportance of the coupling can also be seen from the probability densities $|\psi(x,z)|^2$ of figure 3, computed numerically by inserting the ansatz of equation (10) into the exact Schrödinger equation (1) with $\lambda = 1$:

(i) The probability densities of bound states with $E < V$ deviate only relatively little from those one would have if the motion in the QW and the magnetic field were completely decoupled; there are only small distortions of the sub-band and harmonic oscillator distributions over the x–z plane. Thus, it still makes sense to label these eigenstates at finite tilt angles by the quantum numbers n and l valid at $\vartheta = 90°$. (For the states with energies above V labelling according to their energetic order is more appropriate.)

(ii) Only relatively few basis functions $\varphi_n(z)$ and $\eta_l(x)$ are needed for the computation of $|\psi|^2$: If the wavefunction has n_0 bulges in the z-direction and l_0 bulges in the x-direction one has to take into account the first $n_0 + 2$ basis functions $\varphi_n(z)$ and the first $l_0 + 2$ basis functions $\eta_l(x)$. More basis functions lead to improvements which cannot be seen within the drawing accuracy of figure 3.

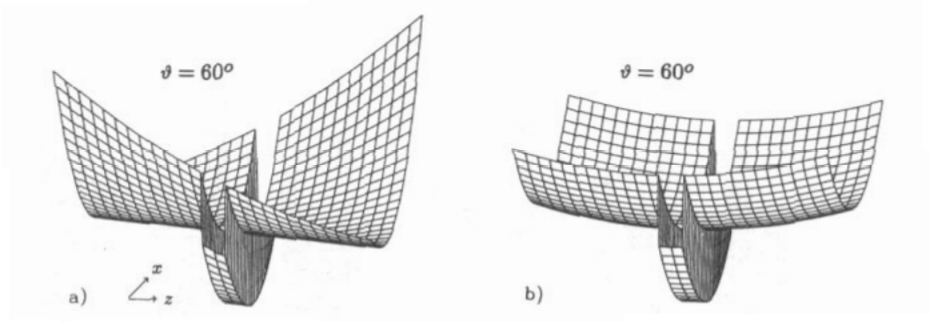

Figure 2. Total potential $W(x, z, \vartheta)$ with (a) and without (b) the coupling H_{xz} at $\vartheta = 60°$ for $B = 0.9$ T, $V = 7.6$ meV, $a = 15$ nm.

Examples of quasi-localized states with $E > V$ are shown in figures 4(a)–(c). As in figure 3 the probability density distributions reflect the point symmetry of the Hamiltonian given by equations (2)–(6). As in the case of a parallel magnetic field [2] these localizations are caused by interferences. In figure 1(a) they are situated energetically in the range between 150 and 200 meV. There the spectrum exhibits small energy gaps which are essentially due to size quantization in the heterojunction of finite width $2L_z$.

The density of states (per unit area) is calculated numerically from

$$g(E) = \frac{2}{2L_x 2L_y} \sum_{nlk_y} \delta(E - E_{nl}) \tag{13a}$$

$$= \frac{2}{2L_x 2L_y} \frac{2L_y}{2\pi} \sum_{nl} \int \mathrm{d}k_y \, \delta(E - E_{nl}) \tag{13b}$$

$$= \frac{2}{2L_x 2L_y} p \sum_{nl} \delta(E - E_{nl}) \tag{13c}$$

where $2L_x 2L_y$ is the cross section of the heterojunction and the factor 2 counts the spin states. Here we have used the fact that E_{nl} is degenerate in k_y so that

$$2\frac{2L_y}{2\pi} \int \mathrm{d}k_y \, \delta(E - E_{nl}) = \delta(E - E_{nl}) 2L_y \frac{eB_z}{\pi\hbar} \int_{-L_x}^{L_x} \mathrm{d}x_0 = p\delta(E - E_{nl}) \tag{14}$$

with

$$p := 2L_x 2L_y \frac{eB_z}{\pi\hbar} \tag{15}$$

being the degeneracy factor. The resulting density of states is shown in figure 5 for two tilt angles. The density of states $g(E)$ at tilt angle $\vartheta = 20°$ recalls the stepwise density of states of a quasi-two-dimensional electron gas at $\vartheta = 0°$, whereas for $\vartheta = 60°$ $g(E)$ indicates the approach to the Landau level structure as $\vartheta \to 90°$.

4. Magnetization

With the numerically calculated energy spectrum E_{nl} shown in figure 1(a) we compute the thermodynamic potential

$$\Omega = -2k_B T \sum_{nlk_y} \ln\left(1 + \exp\left(\frac{\mu - E_{nl}}{k_B T}\right)\right). \tag{16}$$

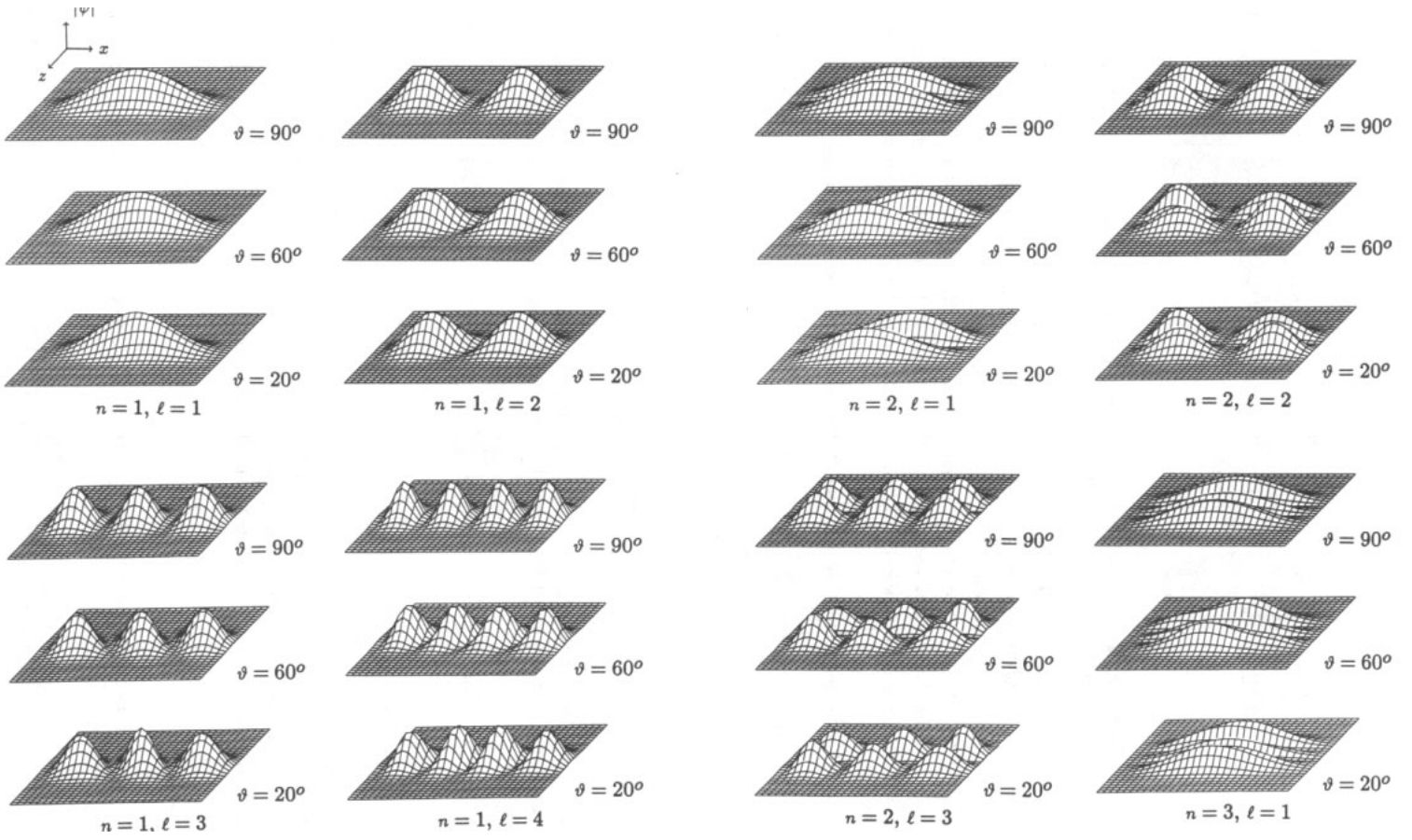

Figure 3. Probability density distributions over the x–z plane of states with energies below V for various n, l. The plots extend between $-a \leqslant z \leqslant a$, $-5a \leqslant x \leqslant 5a$.

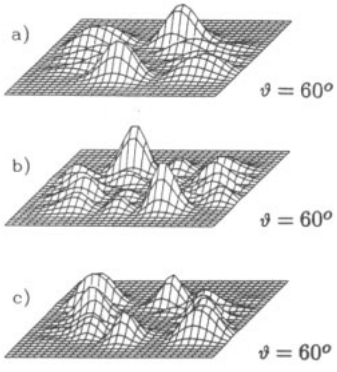

Figure 4. Probability density distributions of states with energies above V at $\vartheta = 60°$ localized essentially (a), (b) in the barrier or (c) on a contour around the minimum of the total potential $W(x, z, \vartheta)$.

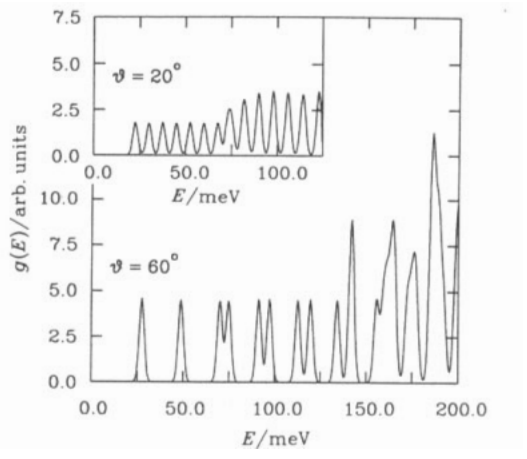

Figure 5. Density of states $g(E)$ for $\vartheta = 20°$ and $\vartheta = 60°$ calculated from equation (13) with the delta functions being replaced by Gaussians of line width 2 meV.

The x and z components M_x and M_z of the magnetization at temperature T and chemical potential μ result from

$$M_{x,z} = -\left(\frac{\partial \Omega}{\partial B_{x,z}}\right)_{v,\mu,T,B_{z,x}=\text{constant}} \tag{17a}$$

$$= 2\sum_{nlk_y} \frac{1}{1+\exp((E_{nl}-\mu)/k_B T)}\left(-\frac{\partial E_{nl}}{\partial B_{x,z}}\right) \tag{17b}$$

$v = 2L_x 2L_y 2L_z$ is the volume of the sample. The integration over k_y is performed as in equation (13) and, for the sake of simplicity, we only consider the temperature $T = 0$ K. We obtain the magnetization per unit area

$$-\frac{M_{x,z}}{2L_x 2L_y} = \frac{eB_z}{\pi\hbar}\sum_{nl}\Theta(\mu - E_{nl})\frac{\partial E_{nl}}{\partial B_{x,z}} \tag{18}$$

where $\Theta(\mu - E_{nl})$ is the step function. The results of the numerical evaluation of equation (18) are shown in figures 6(a)-(c).

The smooth oscillations of the magnetization in a parallel field (figure 6(a)) are very similar to the ones discussed and explained in [1]. The only difference is the drop of the second oscillation minimum to the $M_x = 0$ level. This effect is caused by the finite thickness $2L_z$ of the heterojunction. (The electrons in higher energy levels penetrate deeper into the GaAs barrier and feel the infinite surface potential walls. This gives rise to a magnetization similar to that of an infinitely deep QW.) The first (second) oscillation corresponds to the population of the states in the first (first and second) sub-band, where the decrease is due to the second (negative) term in

$$\frac{\mathrm{d}E_n(z_0)}{\mathrm{d}B_x} = \left.\frac{\partial E_n}{\partial B_x}\right|_{z_0} - \frac{z_0}{B_x}\left.\frac{\partial E_n}{\partial z_0}\right|_{B_x}. \tag{19}$$

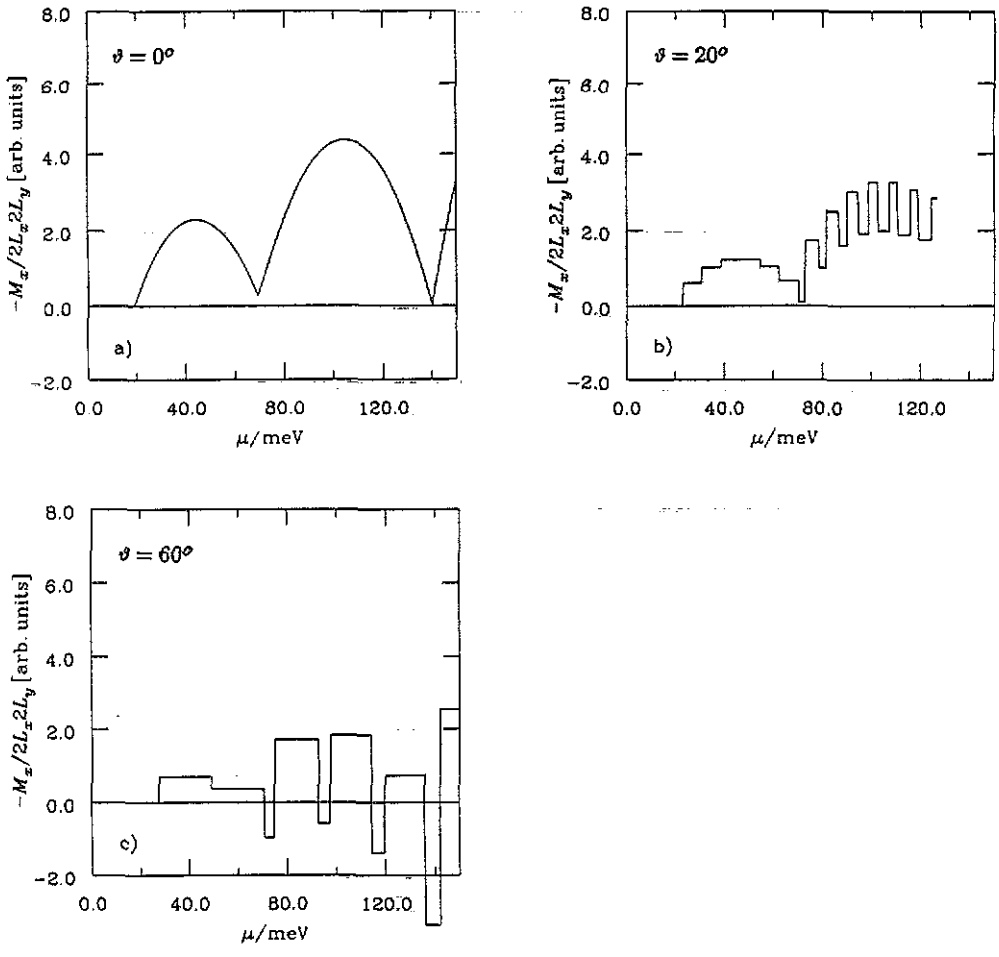

Figure 6. Oscillating negative magnetization per unit area $-M_x/2L_x2L_y$ at various tilt angles ϑ as a function of the chemical potential μ at $B = 15$ T. The QW is $a = 15$ nm wide, the width of the heterojunction is $2L_x = 7a$ and the barrier height is $V = 147$ meV.

Note that in the case of a parallel field $\boldsymbol{B} = \boldsymbol{e}_x B_x$ the quantum number l in (18) is replaced by the quantum number $z_0 = \hbar k_y/eB_x$.

At finite tilt angles the shift of an energy level E_{nl} with the magnetic field component B_α, $\alpha = x, y$, is given by

$$\frac{\partial E_{nl}}{\partial B_\alpha} = \frac{\partial E_{nl}}{\partial B}\bigg|_\vartheta \frac{\partial B}{\partial B_\alpha}\bigg|_\vartheta + \frac{\partial E_{nl}}{\partial \vartheta}\bigg|_B \frac{\partial \vartheta}{\partial B_\alpha}\bigg|_B \tag{20}$$

so that

$$\frac{\partial E_{nl}}{\partial B_z} = \frac{1}{\sin\vartheta}\frac{\partial E_{nl}}{\partial B}\bigg|_\vartheta + \frac{1}{B\cos\vartheta}\frac{\partial E_{nl}}{\partial \vartheta}\bigg|_B \tag{21}$$

$$\frac{\partial E_{nl}}{\partial B_x} = \frac{1}{\cos\vartheta}\frac{\partial E_{nl}}{\partial B}\bigg|_\vartheta - \frac{1}{B\sin\vartheta}\frac{\partial E_{nl}}{\partial \vartheta}\bigg|_B . \tag{22}$$

Since $\partial E_{nl}/\partial B > 0$ always and $\partial E_{nl}/\partial \vartheta > 0$ nearly always, $\partial E_{nl}/\partial B_z$ is always positive, and the magnetization M_z increases (stepwise) with μ. We do not bother to show it here. Much more interesting is the variation of the magnetization $-M_x$ shown in figures 6(*b*) and (*c*). At $\vartheta = 20°$ the first oscillation of the $\vartheta = 0°$ case is still 'remembered'. The steps occur whenever the chemical potential moves through one of the energy levels E_{1l} of figure 1(*a*). With increasing l, $\partial E_{1l}/\partial \vartheta$ increases so that the negative contribution to $\partial E_{1l}/\partial B_x$ in equation (22) gains more and more weight and finally leads to the decrease of $-M_x$ according to equation (18). As the chemical potential moves across the lowest branch E_{2l} of the second Landau fan, $\partial E_{2l}/\partial \vartheta$ is small and $-M_x$ rises again. The next branch to be crossed by μ, however, originates from the first Landau fan with $n = 1$ and $l = 8$. Its ϑ derivative in equation (22) is large, and the negative magnetization drops drastically. The following level to be crossed again belongs to the $n = 2$ set, the ϑ derivative is small, and the magnetization jumps up. This rise and fall continues as the the chemical potential moves through the alternating levels from different Landau branches. The same story is basically true at $\vartheta = 60°$, figure 6(*c*); the $\vartheta = 0°$ case is hardly 'remembered', and the wider gaps between the branches in figure 1(*a*) are reflected by wider separations between the jumps in the magnetization.

5. Discussion

There are degenerate localized states above the barrier edge of a QW within a finite size heterojunction in a tilted magnetic field. Their energies may be separated by small energy gaps from the rest of the spectrum. This separation, however, is essentially an effect of size quantization and increases with decreasing width $2L_z$ of the heterojunction. The degeneracy increases proportional to the perpendicular field B_z and may favour overpopulation at certain energies under appropriate 'pumping' conditions. Nevertheless we are sceptical whether a sufficiently strong non-equilibrium distribution of electrons—which would be the basis for a magnetically tunable laser—can be produced. Far more interesting from a technological point of view are the sharp jumps of the magnetization as a function of the chemical potential in tilted fields. They could provide the 'yes–no' elements of a dissipation free switching device. Although our calculations have been performed so far for rectangular QWs only, we are quite positive that magnetization jumps will also occur in MOSFETs in tilted fields where the chemical potential can be shifted easily by changing the gate voltage. Finite temperatures will soften the jumps somewhat. The main problem is how the jumps will be influenced by many-body effects. This is the subject of ongoing research.

Acknowledgments

All numerical calculations have been done on the VAX 8810 and VAX 6000-420 of the Rechenzentrum der Universität Würzburg.

References

[1] Huckestein B and Kümmel R 1988 *Phys. Rev.* B **38** 8215

[2] Marx G, Huckestein B and Kümmel R 1991 *J. Phys.: Condens. Matter* **3** 6425
[3] Johnson E, MacKinnon A and Goebel C J 1987 *J. Phys. C: Solid State Phys.* **20** L521
[4] Johnson E and MacKinnon A 1988 *J. Phys. C: Solid State Phys.* **21** 3091
[5] Maan J C 1984 *Springer Series in Solid State Science* vol 53 (Berlin: Springer) p 183
[6] Haydock R, Heine V and Kelly M J 1972 *J. Phys. C: Solid State Phys.* **5** 2845
[7] Lee H J, Luravel L Y, Woolley J C and SpringThorpe A J 1980 *Phys. Rev.* B **21** 659